SMALL-SCALE ROTOR EXPERIMENTS WITH ON-BLADE ELEVONS TO REDUCE BLADE VIBRATORY LOADS IN FORWARD FLIGHT

Mark V. Fulton

and

Robert A. Ormiston

Aeroflightdynamics Directorate
US Army Aviation RD&E Center (AMCOM)
Ames Research Center
Moffett Field, California

Abstract

A low-tip-speed 7.5-ft diameter hingeless rotor with one on-blade elevon control surface on each of the two blades was wind tunnel tested for advance ratios from 0.1 to 0.3 at two rotor speeds (450 and 760 RPM) and at low to moderate thrust coefficients. The purpose of this study was to investigate dynamic response characteristics and to determine the effectiveness of on-blade elevon control to reduce blade vibratory loads. Dynamic response characteristics were investigated at high advance ratios up to 0.6 for non-thrusting conditions. All elevon excitations were open loop. Primary measurements included elevon deflection and blade root flap bending and torsion moments. The tests successfully demonstrated the effectiveness of on-blade elevon controls for significantly reducing or canceling individual 3, 4, and 5/rev harmonic blade vibratory flap bending moments at representative forward flight advance ratios. Elevon effectiveness determined from complementary discrete frequency and continuous frequency response function measurements affords a very useful means of evaluating the potential influence of tailoring structural dynamic and aeroelastic effects to reduce vibratory loads.

Introduction

There has long been a desire to reduce helicopter vibration. Traditional approaches have been based on optimizing the rotor and fuselage structure to minimize response to unsteady aerodynamic excitation, or installing vibration absorbers or isolators in the rotor or fuselage. Unfortunately, these techniques can have limited effectiveness and add nonproductive weight to the rotorcraft. In addition, the "jet-smooth ride" still eludes helicopter designers. Consequently, considerable effort is now being directed toward on-blade aerodynamic control concepts in the hopes of further reducing vibration for low weight and low power. The present investigation uses a trailing-edge control surface, or elevon, to generate local aerodynamic lift and pitching moment for vibration reduction. The term elevon is used herein for simplicity and clarity since other terms, such as flap, aileron, and servo-flap, have multiple meanings.

Analytical investigations by Millott and Friedmann, Refs. 1 and 2, and Milgram and Chopra, Refs. 3 and 4, have shown that the active elevon control concept is theoretically practical for reducing rotor vibratory forces and moments transmitted to the fixed system. That is, with one elevon per blade, and for practical deflection amplitudes, vibration reduction is comparable to HHC blade pitch. Moreover, the elevon actuator power is significantly less than the HHC power required to pitch the entire blade. These studies also included preliminary investigations of optimizing the structural dynamic properties of the blade such as torsion frequency placement and elevon location.

Forward flight testing of on-blade elevon concepts has been limited. Consequently, there remains much that is unproven and poorly understood about these concepts. The earliest related wind tunnel test appears to be the full-scale Kaman Multicyclic Controllable Twist Rotor (MCTR), which was tested in the NASA Ames 40- by 80-Foot Wind Tunnel in 1976, Refs. 5 and 6. This test used electrohydraulic actuators in the rotating system to drive the servo-flap control surface at 2/rev - 4/rev. Only limited test results for vibratory load reductions were achieved. Another previous wind tunnel test was the McDonnell Douglas Active Flap Rotor (MDAFR) test conducted in the NASA Langley 14- by 22-Foot Subsonic Tunnel in 1994, Ref. 7. This rotor was designed to investigate acoustic noise reduction and used an on-blade elevon with hub-mounted cam actuation. In keeping with the acoustic objectives of the investigation, the structural dynamics of the model did not represent typical rotor blade characteristics. Vibration testing was limited to a harmonic of 5/rev.

Presented at the American Helicopter Society 54th Annual Forum, Washington, DC, May 20-22, 1998.

The model used for the present study was previously tested in the Aeroflightdynamics Directorate Hover Test Chamber as reported in Ref. 8. This model is a low-tip-speed 7.5-ft diameter hingeless rotor with one on-blade elevon control surface on each of the two blades. The construction is relatively simple to minimize cost, but the dynamic characteristics are sufficient to permit exploratory investigation of a number of fundamental aeroelastic, structural dynamic, and vibratory load response characteristics pertinent to advanced active control rotor concepts. Hover testing of this rotor, including quasi-steady and dynamic test results for nonrotating and rotating conditions, was reported in Ref. 8.

The purpose of the present study was to investigate forward flight dynamic response characteristics and to determine the effectiveness of elevon control in reducing blade vibratory moments. The rotor was tested in forward flight for advance ratios from 0.1 to 0.3 at low to moderate thrust coefficients. All elevon excitations were open loop. Primary measurements included elevon deflection and blade root bending and torsion moments. An ability to control these blade moments is an indication that vibratory hub loads could also be controlled. Additional testing was performed for non-thrusting conditions (0 deg collective pitch) for advance ratios up to 0.6 to more effectively investigate the effects of forward flight on the dynamic response characteristics. Results of forward flight wind tunnel testing will be presented herein.

Experimental Model

A low tip-speed (298 ft/sec), small-scale dynamic model of low cost and complexity was suitable for this exploratory investigation. The model is shown in Fig. 1 installed on the Small Scale Rotor Test Rig (RTR) in the Army/NASA 7- by 10-Foot Wind Tunnel.

The 7.5-ft diameter rectangular, untwisted rotor blades are uniform in mass and stiffness except at the blade root and the elevon "active section". Chordwise mass and aerodynamic centers are located near the quarter chord of the symmetrical NACA 0012 airfoil section. The blades are constructed of composite materials including a fiberglass spar, foam core, and fiberglass wrapped skin construction. Each blade has two bimorph actuators driving a single, 10% chord, plain elevon with a span of 12% blade radius, centered at the 75% radial location. The two piezoceramic, lead zirconate titanate (PZT), bimorph bender beam actuators are cantilevered to the rear of each blade spar. Fiberglass lever arms project forward from the elevon to engage the tip of the cantilever PZT beam to produce elevon rotational motion, Fig. 2. A photograph of the actuator and elevon installation is shown in Fig. 3. Model physical properties and operating conditions are listed in Table 1 and additional design and construction details of the blades, actuators, and elevons are available in Ref. 8.

Elevon motion was measured with a Hall-effect transducer and blade moment responses were measured through full strain gage bridges at the root flexure of each blade. The flap and chord strain gage bridges were at 0.114 R, and the torsion strain gage bridge was at 0.128 R. In addition, the root pitch of blade 1 was measured with a potentiometer. Although not discussed in this paper, PZT voltage and current were also measured to provide data on actuator power. This data is reported in Ref. 8 for hover.

Rotor Blade Structural Dynamic Characteristics

The calculated rotor blade frequency fan plot (in air at 0 deg collective pitch), Fig. 4, illustrates the structural dynamic characteristics of the rotor blades. The frequencies were predicted by Second Generation Comprehensive Helicopter Analysis System (2GCHAS), Ref. 9, using blade properties adjusted to match measured nonrotating frequencies. The nominal rotor speed (760 RPM, 12.7 Hz) results in a representative first-flap frequency of 1.11/rev. The rotor is stiff inplane, with a first lead-lag frequency of 1.08/rev, and was somewhat sensitive to 1/rev loads. The second flap bending mode is above 3/rev unlike most rotor blades, where this mode is below 3/rev. The first torsion frequency is 4.6/rev. Both the first elevon/actuator and third flap bending frequencies are between 6/rev and 7/rev at nominal rotor speed. The bimorph/elevon fundamental natural frequency was estimated assuming quasi-static 2-D airfoil aerodynamics and ignoring mechanical friction.

At the alternative 450 RPM rotor speed used in the present investigation, the principal blade (nondimensional) natural frequencies are much increased and consequently are unrealistic compared to typical rotor blades. The second flap and first torsion frequencies are above 4/rev and 7/rev, respectively. Nevertheless, this change in natural frequencies affords an opportunity to broaden, in some respects, the fundamental understanding of on-blade elevon control and vibration reduction characteristics.

Synopsis of Previous Hover Test Data

As an introduction to the present forward flight vibratory loads reduction investigation, it will be useful to summarize in this section the principal results of previous hover testing of the rotor used in the present investigation. Additional details can be found in Ref. 8.

The small-scale active rotor demonstrated the feasibility of using piezoceramic bimorph actuators (at low tip speeds) to provide reasonable elevon deflections of ± 10 deg nonrotating and ± 5 deg up to 4/rev at the nominal rotor speed of 760 RPM.

Low-frequency blade torsion moment response to elevon deflection indicated that elevon effectiveness was lower than predicted by thin airfoil theory, largely due to the effects of low Reynolds number on elevon control power, $c_{m\delta}$.

Low frequency blade root flap bending response exhibited an "elevon reversal speed" slightly above 760 RPM, due to elastic blade twist induced by the negative elevon aerodynamic pitching moment.

Aeroelastic and structural dynamic response characteristics were evaluated over a wide rotor speed range using frequency sweep excitation of the elevon up to 105 Hz (8/rev at 760 RPM). CIFER® (Refs. 10 and 11) was used to calculate the frequency response function magnitude, phase and coherence of measured blade flap bending and torsion moments to elevon input and elevon response to actuator input voltage.

Frequency response functions indicated that blade torsion moment response at resonance was amplified approximately five times the steady-state amplitude.

Blade flap bending responses produced by the available range of elevon deflection suggested that it would be possible to achieve significant reductions of anticipated 3, 4, and 5/rev vibratory flap bending moments in forward flight. The success of these hover tests led directly to the forward flight testing reported herein.

Superposition Model

The basic on-blade control concept of reducing rotor vibratory loads in forward flight is that aerodynamic induced blade loads, which are generated by a particular frequency of elevon excitation (at an integer harmonic of the rotor rotational frequency), will cancel the steady-state periodic load at the same frequency if the amplitude and phase of the elevon excitation are properly selected. This requires, of course, that the elevon be capable of inducing a blade load of sufficient magnitude to cancel the steady-state blade load. A simple superposition model will be introduced to illustrate this basic effect and will be employed later to assist in evaluating the experimental results.

If periodic response is assumed, with the fundamental period equal to one rotor revolution, then the steady-state vibratory moment (for zero elevon motion) can be represented as

$$Ms = Ms_o + \sum_{i=1}^{n} Ms_i * Cos(i\psi + \phi_{Msi}) \qquad (1)$$

where Ms_o is the mean, and Ms_i and ϕ_{Msi} are the amplitude and phase of the i^{th} harmonic. The same form can be used for both the elevon-induced moment, $M\delta$, and the total resultant moment, Mt. If the rotor is assumed to respond linearly, then superposition can be invoked, giving

$$Mt = Ms + M\delta \qquad (2)$$

In this case, the amplitude of the ith harmonic of the total vibratory moment, Mt_i, can be shown to be a function of the steady-state and elevon-induced moments:

$$Mt_i = \sqrt{Ms_i^2 + 2 * Ms_i * M\delta_i * Cos(\phi_{Msi} - \phi_{M\delta i}) + M\delta_i^2} \qquad (3)$$

The behavior of this superposition model is illustrated in Fig. 5, where the amplitude of the total response for the ith harmonic (Mt_i) is plotted as a function of the phase of the elevon-induced moment ($\phi_{M\delta i}$) for zero deg phase of the steady-state moment (ϕ_{Msi}) and for various amplitudes of the elevon-induced moment ($M\delta_i$). Note that for this illustrative example, the amplitude of the elevon-induced moment is assumed to remain independent of the phase of the elevon excitation. This assumption will be invoked for analysis of the experimental data presented below, and is a reasonable approximation for a rotor blade where the effects of forward flight aerodynamics are relatively modest at low and moderate advance ratios.

This figure illustrates two principal effects. First, both "underdriven" and "overdriven" conditions are shown, where the excitation input is either insufficient or excessive for countering the steady-state response, respectively. Second, cancellation is shown to require 180 deg phasing of the elevon-induced moment relative to the steady-state moment.

Wind Tunnel Test Procedures

Forward flight testing was conducted in the Army/NASA 7- by 10-Foot Wind Tunnel. Testing was performed at 760 and 450 RPM, with 760 being the "nominal" rotor speed. All of the data in this paper is for a shaft angle of zero deg. Trim conditions were established using a wind tunnel trim procedure which used cyclic pitch control to minimize the 1/rev flap bending moment for blade 1. Filter corrections have been made to remove the effects of electronic filtering.

Forward flight testing of the rotor model in the wind tunnel used four primary test methods: 1) steady-state testing to establish baseline vibratory loads (for zero applied voltage) and establish the useable wind tunnel test envelope, 2) elevon phase sweeps (at constant PZT voltage harmonic) to investigate the effect of the phase of elevon motion on vibratory loads and determine elevon effectiveness at discrete elevon harmonics, 3) PZT voltage sweeps to investigate the effect of elevon motion amplitude on vibratory load cancellation, and 4) elevon frequency

sweeps to measure rotor frequency response functions for blade root flap bending and torsion moments. Details of the test procedures as well as the results obtained for each test method will be described in later sections.

Discussion of Results

Steady-State Blade Loading

Steady-state data was obtained to quantify the variation of the blade root vibratory loads with flight speed (for zero applied PZT voltage). The steady-state test envelope is shown in Fig. 6 for both 760 and 450 RPM at a range of advance ratios (μ) from 0 to 0.3. Since at 760 RPM the maximum achievable collective pitch (θ_o) was constrained by allowable blade loads to be only 4 deg, testing was also performed at 450 RPM. This reduced rotor speed not only allowed testing to a higher nondimensional rotor thrust loading (thrust coefficient/solidity) but also changed the blade natural frequencies (as shown in Fig. 4). Figure 7a illustrates the nondimensional rotor thrust loading reached during testing as predicted using 2GCHAS (at 760 RPM). The lower curve is at 4 deg collective pitch and represents the maximum thrust achieved at 760 RPM. The upper curve is at 6 deg collective pitch and is similar to the maximum collective obtained at 450 RPM. This upper curve shows that a nondimensional rotor thrust loading in excess of 0.06 was achieved at 450 RPM for most of the advance ratios tested.

Figure 7b shows the variation of the mean flap bending moment with advance ratio at the maximum collective pitch for each rotor speed. The trends are similar to the thrust curves (Fig. 7a) and both rotor speeds are shown to produce similar dimensional loads. If these results were nondimensionalized by rotor speed, however, the 450 RPM results would be larger than those at 760 RPM.

The effect of advance ratio on the 2/rev - 5/rev harmonics of the steady-state vibratory blade 1 root flap bending moments is shown in Figs. 7c and 7d for 450 RPM and 760 RPM, respectively. The multiple data points indicate scatter due to flow unsteadiness and variations in the cyclic trim settings. Each plot has curves which indicate the average trend for each harmonic. These plots are included primarily to indicate the baseline vibratory load levels experienced by the rotor and thus identify the magnitude of vibratory load alleviation needed for on-blade elevon control to be considered viable as a vibration reduction concept.

Note that a comparison of the steady-state vibratory blade loads for the two rotor speeds indicates that the 2/rev flap moment harmonic is higher at 450 RPM while the 3/rev component is higher at 760 RPM. The 2/rev behavior is likely due to the higher dimensionless rotor thrust loading at 450 RPM; the 3/rev behavior, however, is likely due to the proximity of the second flap bending frequency to 3/rev at 760 RPM.

Elevon Phase Sweeps

Phase sweeps of elevon motion were performed to investigate the effect of the phase of elevon motion on vibratory loads and to determine elevon effectiveness at discrete elevon harmonics. First, a trimmed flight condition was established, including shaft angle, rotor speed, advance ratio, and collective pitch, with cyclic pitch adjusted to minimize the 1/rev flap bending moment of blade 1. Next, a discrete integer harmonic of the rotor speed (from 1/rev to 5/rev) was chosen for harmonic PZT voltage excitation (at a constant voltage amplitude). A phase sweep of the PZT voltage was then performed, acquiring a data point for a series of elevon phase angles (at constant cyclic pitch). The collective pitch used for each voltage harmonic and advance ratio is given in Table 2 for 760 RPM. For 450 RPM, all phase sweeps were at an advance ratio of 0.2 and a collective of 6.25 deg. This phase sweep data provides a measurement of elevon effectiveness and identifies the elevon phase required to minimize a flap bending moment harmonic.

For each test point, the amplitude of the response is obtained using an FFT of the response at the frequency of the applied voltage. These are the "direct" responses. In each case, the amplitudes for each individual blade are plotted versus the phase of the corresponding individual elevon. That is, blade 1 results are plotted versus the phase of elevon 1, and blade 2 results are plotted versus the phase of elevon 2.

Direct Responses for Five Voltage Harmonics

Phase sweep results are shown in Figs. 8a - 8f for a 760 RPM case (θ_o = 4 deg, and μ = 0.2). Figure 8a shows the variation of the 5/rev amplitude of the elevon angle for a 5/rev voltage excitation. Note that this figure shows only a small variation in the elevon amplitude with phase. This is similar to other harmonics and indicates that the elevon motion was relatively constant for the phase sweeps.

Figures 8b - 8f show how the flap bending moment amplitudes vary with elevon phase for 1/rev - 5/rev voltage excitation, respectively. Here, the straight lines indicate the baseline steady-state amplitudes for zero excitation voltage. The data points represent the total bending moment at different elevon phases for a sinusoidal excitation voltage between 66 and 110 Vrms, depending on the harmonic. (The voltage level was adjusted for each harmonic to generate a large change in the flap bending response without exceeding the allowable blade loads.) In each of these five cases, there is a large change in the total flap bending moment amplitude which is caused by the elevon-induced moment ($M\delta$). Note that although the two blades

show significantly different baseline uncontrolled responses, which are likely caused by structural and aerodynamic differences between the two blades, both blades show significant sensitivity to the elevon motion. It is the elevon-induced moment which explains not only the variation of the bending moment amplitude with elevon phase, but also the increase in the mean during overdrive conditions (as seen in Figs. 8e and 8f for the 4/rev and 5/rev cases). Also note that the 3/rev elevon motion provides a nearly complete cancellation of the 3/rev flap bending moment for a phase of about 90 deg (Fig. 8d).

The figures include curve fits of the data points based on the superposition model of Eq. 3, with the magnitude and phase of each baseline flap bending moment harmonic (Ms_i and ϕ_{Msi}) specified; the remaining variables, the amplitude and phase of the elevon-induced moment ($M\delta_i$ and $\phi_{M\delta i}$), were left as free parameters to be identified from the measured data. With the exception of the 1/rev case, this approach provides good results as can be judged from the quality of the identified curve fits included in the figures.

Summary of Elevon-Induced Moments

The phase sweep data for an advance ratio of 0.2 was processed as described in the previous section for two rotor speeds, 450 RPM and 760 RPM (θ_o = 6.25 and 4 deg respectively). This data processing yielded the direct, elevon-induced flap and torsion moments for 1/rev - 5/rev applied voltages. These results are summarized in this section for blade 1 and presented in the form of bar charts in Figs. 9a - 9d. Both the uncontrolled baseline harmonics (Ms_i) and the elevon-induced harmonics ($M\delta_i$) of flap bending and torsion moment are plotted for 450 RPM in Figs. 9a - 9b (and for 760 RPM in Figs. 9c - 9d). For ease of comparison, each harmonic of the elevon-induced moments has been scaled for ± 5 deg elevon motion (assuming linearity).

Consider first the flap bending moments at 760 RPM, Fig. 9c. Comparing the amplitudes of each elevon-induced harmonic to its corresponding uncontrolled (baseline) harmonic provides an indication of elevon effectiveness with respect to its capability for canceling that baseline vibratory load. At this flight condition (μ = 0.2, and θ_o = 4 deg), elevon effectiveness is sufficient to cancel the flap bending moment at all harmonics except 2/rev.

The corresponding torsion moment results for 760 RPM (Fig. 9d) show elevon-induced moments more than twice as large as the uncontrolled (baseline) torsion moments (for 2/rev - 5/rev). This indicates that for ± 5 deg elevon motion at 2/rev - 5/rev, the amplitude of blade torsion moment would be increased, regardless of the phasing of the elevon motion. This could be considered to be a "control cost" for this on-blade control concept. In future embodiments of this concept, this "control cost" could appear as increased blade loads for vibratory hub loads reduction.

A comparison of elevon-induced torsion moments for rotor speeds of 450 RPM and 760 RPM, in Figs. 9b and 9d, respectively, illustrates that, for the same ± 5 deg elevon motion, the effect of increasing dynamic pressure is manifested as a corresponding increase in elevon-induced moment. This increased torsion motion can be expected to increase the resultant blade dynamic twist and thereby indirectly influence flap bending moments. The effect of elevon direct lift, however, must also be taken into consideration (see Ref. 8 for additional details).

The flap bending moment results for 450 RPM (θ_o = 6.25 deg) in Fig. 9a show reduced elevon effectiveness (relative to the 760 RPM results in Fig. 9c). This difference can be attributed to several related factors. First, the increased dimensionless rotor thrust loading at the higher collective pitch generally increases baseline vibratory airloads acting on the blades. Second, the baseline vibratory loads depend on the blade dynamic response characteristics. Third, the elevon-induced moments are also influenced by the RPM-dependent structural dynamics. Note, for example, the significant reduction in effectiveness at the 3/rev harmonic frequency. And fourth, the reduced dynamic pressure reduces the elevon torsion moment effectiveness noted above. It may be noted that, although the results presented in Fig. 9 were scaled for ± 5 deg elevon motion, significantly larger elevon motions were achieved at 450 RPM due to the lower dynamic pressure.

In summary, it is of interest to note the large variations in the elevon-induced moments from one harmonic to the next as well as the dramatic differences in flap and torsion moment response characteristics. Furthermore, the trends change significantly between 450 and 760 RPM. These differences are caused by aeroelastic and structural dynamic effects and will be discussed below in conjunction with the frequency sweep results.

PZT Voltage Sweeps

For several selected flight conditions, PZT voltage sweeps were performed (at a fixed harmonic) with the elevon phase chosen to achieve cancellation of the baseline blade loads (for sufficiently large elevon motions). To first order, the PZT voltage sweeps are equivalent to elevon amplitude sweeps. Before discussing these results, however, projections of the effects of elevon angle amplitude will be made using the elevon-induced moments extracted from the phase sweep results. Later in this section, these projections will be compared to the voltage sweep data.

Projections Using Phase Sweep Data

The measured flap bending moment response characteristics derived from the phase sweep curve fits will now be used to project how vibratory loads vary as a function of elevon amplitude for blade 1. These projections will be performed using the uncontrolled and elevon-induced data shown in Figs. 9a and 9c.

To begin, assume that the elevon-induced moment is proportional to elevon angle. Next, assume that the phase of the elevon motion is chosen to minimize the total response. For a given harmonic, the uncontrolled (or steady-state) response (Ms) can then be used with the elevon-induced moment (Mδ) to project the variation of the total response (Mt) with elevon angle (δ):

$$Mt_n = \left| Ms_n - \left(\frac{M\delta_n}{5^\circ} \right) * \delta \right| \qquad (4)$$

where 5 deg is used to normalize $M\delta_n$ because the elevon motion chosen for Figs. 9a and 9c was ± 5 deg. Equation 4 indicates that the (total) flap bending moments are reduced for an increasing elevon deflection amplitude until cancellation is achieved; for larger elevon motions, an "overdriven" condition begins, causing the total response to increase from zero.

Figures 10a and 10b show the effect of the amplitude of elevon motion on various (total) flap bending moment harmonics for an advance ratio of 0.2 and rotor speeds of 450 RPM (θ_o = 6.25 deg) and 760 RPM (θ_o = 4 deg), respectively. The projections from Eq. 4 are shown as lines in these two figures. In each plot, the data for Eq. 4 was taken from Figs. 9a and 9c. The point at which each line intersects zero flap moment indicates the projected amplitude of elevon motion needed for complete cancellation of that particular flap bending harmonic.

Comparison of Voltage Sweep Data with Projections

Also plotted in Figs. 10a and 10b are data points obtained from voltage sweeps. For Fig. 10a (450 RPM), two voltage sweeps were performed – 4 and 5/rev. For Fig. 10b (760 RPM), three voltage sweeps were performed – 3, 4, and 5/rev. In each of these five cases, the data points follow the general trend of the projections. The main discrepancy is the vertical offset between the projections and the data points. This offset is caused by a change in the uncontrolled (steady-state) response from one test run to the next. This change was likely due to a change in the flight condition (collective and cyclic pitch changes, e.g.) between the phase sweeps (used for the projections) and the voltage sweeps (shown as discrete data points).

Finally, note the different axis scalings used for Figs. 10a and 10b. Using the 4/rev cases as an example, notice that similar uncontrolled amplitudes exist and that the elevon effectiveness is reduced at 450 RPM. Also note, however, that significantly larger elevon motions were achieved at 450 RPM, permitting a sizable reduction in the 4/rev flap bending moment.

An Example of Vibration Reduction

An illustrative example of vibration reduction will now be briefly explained (using blade 1 results). This example uses two data records from the 760 RPM (θ_o = 4 deg, μ = 0.2) voltage sweep depicted in Fig. 10b. Consider two data points on Fig. 10b. The first data point is one of the steady-state test conditions (with zero applied voltage). The second data point corresponds to an elevon motion of about two deg (with 42.6 Vrms applied voltage) and yields the minimum 4/rev flap bending amplitude shown on Fig. 10b.

First, consider the elevon motion, which was reconstructed from the mean and the first twelve harmonics of the time history. The resultant azimuthal time history shown in Fig. 11 illustrates several features of the elevon motion. The elevon motion shown for the uncontrolled baseline case is very small, as would be expected. For the controlled case, however, large 4/rev elevon motion exists, along with moderate 1/rev content as well as other harmonics. The 1/rev content is due in part to the azimuthal variation of elevon aerodynamic "stiffness" opposing the PZT actuator deflection. Although multi-harmonic elevon motion complicates interpretation (as will be shown below), the dominant effects are still evident.

For example, the desired effect of significantly reducing the 4/rev flap bending moment was accomplished as shown in Fig. 12. The fact that flap harmonics other than 4/rev are affected is likely caused by the multi-harmonic elevon motion, and to a reduced degree at this advance ratio (μ = 0.2), by interharmonic coupling induced by the periodic coefficients of forward flight.

Side Harmonic Effects

Side Harmonic Elevon Motion

As described in the previous section, the amplitudes of the elevon motion were appreciable at some neighboring rotor harmonics of the applied voltage frequency. In this section, blade 1 results will be used to further illustrate this extraneous elevon motion; the resultant flap bending response will be described in the next section. The flight condition is for 760 RPM, 2 deg collective pitch, and an advance ratio of 0.3. Three PZT voltage excitation harmonics will be examined – 3, 4, and 5/rev.

Figure 13a shows eight harmonics of the induced elevon motion for each of the three voltage harmonic cases (3/rev - 5/rev). In each case, the elevon motion has been normalized to ± 5 deg at the primary harmonic. Note that in each case the elevon harmonics are dominated by the elevon response at the PZT excitation harmonic. Also note that each case has a significant response at the immediate side harmonics of ± 1/rev. For example, the 4/rev case has a 0.8 deg amplitude at 3/rev and a 1.0 deg amplitude at 5/rev. The responses at other nonprimary harmonics are small for these three cases.

The nonprimary (extraneous) elevon harmonics are likely caused by aerodynamic and inertial blade motion coupling effects. These neighboring harmonics remain because a feedback controller was not used to enforce a pure sinusoidal elevon motion. Although this complicates interpretation, the dominant effects are still evident.

Side Harmonic Flap Bending Moment Response

Previous sections have focused on the *direct* induced moments, that is, the amplitude of the flap and torsion moments at the applied voltage harmonic. An example of the side harmonic flap response will now be given. To begin, the first eight harmonics of the elevon-induced moments were calculated in a fashion similar to the calculations for one of the direct responses previously described for Figs. 8b - 8f. These eight harmonics were then normalized to correspond to an elevon motion of ± 5 deg at the primary elevon harmonic.

The induced flap moment harmonics are shown in Fig. 13b for 3/rev - 5/rev voltage excitation cases. These moments correspond to the elevon motions shown in Fig. 13a. Consider the 4/rev case. For the 4/rev voltage excitation, the induced flap moment at 4/rev ($M\delta_4$) has an amplitude of 2.4 in-lb (for an elevon motion of ± 5 deg at 4/rev as shown in Fig. 13a). The induced flap bending responses at other harmonics are clearly not zero. For example, the amplitude at 3/rev ($M\delta_3$) is 0.8 in-lb, or 33% of the 4/rev response. Since the 3/rev elevon motion was 0.8 deg, or 16% of 5 deg, a significant portion of the 3/rev flap response is likely caused by the side harmonic elevon motion. (This argument implicitly invokes aeroelastic/structural dynamic effects which will be described in the next section.) The remainder of the 3/rev flap response, however, remains unexplained but could be caused by unexplained trim changes or, to a small degree, by interharmonic coupling. The amount of interharmonic coupling caused by the periodic coefficients at this advance ratio ($\mu = 0.3$) is likely to be small. Further detailed data analysis and correlation with analytical predictions will be required to better determine the exact cause of the observed side harmonic flap moment responses.

Elevon Frequency Sweeps

As was done for hover testing (Ref. 8), frequency sweeps of elevon excitation were conducted to determine rotor system frequency response functions (FRFs) for blade root flap bending and torsion moments. In forward flight, these FRF studies permit a study of the influence of advance ratio on elevon effectiveness. The FRFs provide a direct means of understanding the fundamental aeroelastic and structural dynamic characteristics of the elevon/rotor blade system. In addition, the continuous FRFs will be compared with the discrete frequency induced moments previously extracted from the elevon phase sweep data.

The frequency sweep data was acquired using logarithmic frequency sweeps from 1 to 105 Hz (in 27 sec). These frequency sweeps were performed for a range of advance ratios (up to $\mu = 0.6$) for the non-thrusting condition (0 deg collective) in order to avoid blade allowable load limits, although some lower advance ratio sweeps were also performed at higher collective pitch angles.

For the frequency sweeps, frequency response functions were obtained using CIFER® (Comprehensive Identification from FrEquency Responses), Refs. 10 and 11. The CIFER® results are presented for average responses (not to be confused with window averaging). The average responses were calculated by averaging the time histories from the two different blades to obtain the response of an "average" blade. These averaged results were processed by the CIFER® module FRESPID (Frequency RESPonse IDentification). FRESPID calculated the FRFs for five different spectral window lengths by concatenating several 30 sec time histories for each test condition. Final signal conditioning included a digital filter with a -3 dB cut-off frequency of 105 Hz. Finally, the CIFER® module COMPOSITE was used to perform multi-window averaging of the FRESPID results. These COMPOSITE results are reported in this section. The FRFs calculated using CIFER® have been converted into dimensional torsion and flap bending moments assuming ± 5 deg elevon motion.

Advance Ratio Effects

The value of the frequency sweep technique is that the aeroelastic/structural dynamic characteristics of the blades can be illuminated. As an example, consider a flight condition at 450 RPM, 0 deg collective pitch, and three advance ratios ($\mu = 0.2$, 0.4, and 0.6). The FRF for the torsion moment generated by elevon motion is plotted in Fig. 14a for elevon frequencies ranging from 1 to 100 Hz. The first torsion natural frequency is well excited at an elevon frequency of about 57 Hz for each advance ratio. The resonant peak is slightly reduced as the advance ratio increases, suggesting an increased amount of aerodynamic

damping with tunnel speed. In addition, the low frequency response (below 5 Hz) changes slightly with advance ratio – the quasi-static torsion moment increases with advance ratio. This trend is understandable since as the advance ratio increases the average dynamic pressure at the elevon is increased.

Figure 14b shows the FRF for flap bending moment, clearly delineating the first three flap bending natural frequencies – the first near 13 Hz, the second near 32 Hz, and the third near 70 Hz. Although the resonances at the second flap mode appear similar for all three advance ratios, there is a significant difference at the third flap natural frequency – the increased flight speed significantly reduces the resonant peak, suggesting a measurable increase in aerodynamic damping.

The low frequency response (below 5 Hz) shows the elevon reversal effect – as the advance ratio increases, the flap bending moment decreases, indicating that the average dynamic pressure is approaching the elevon reversal condition. (In hover, elevon reversal occurred slightly above 760 RPM.) This reversal effect is caused by the increasing aerodynamic pitching moment which is evident in the torsion moment shown in Fig. 14a. As this pitching moment increases, the resultant dynamic twist of the blade increases, creating a lift change which acts in opposition to the direct lift acting on the elevon. This is the elevon reversal effect described in more detail in Ref. 8.

Similar FRFs were attempted for 760 RPM, but the coherence of the flap bending results was sufficiently low to limit their usefulness. On the other hand, the torsion FRFs were acceptable and will be used below. Some use of the 760 RPM flap bending FRFs may be found in the future, but at present it appears that the elevon motion was not sufficiently large to create an adequate signal-to-noise ratio. Here, the "noise" is simply the uncontrolled, or ambient, vibratory response produced by forward flight.

Comparison with Induced Moments from Phase Sweeps

It is of interest to compare the continuous FRF results with the induced moments which were previously extracted from the phase sweeps (performed at discrete frequencies). The first results shown are the torsion moments at an advance ratio of 0.2 for two rotor speeds, 450 RPM (θ_o = 6.25 deg) and 760 RPM (θ_o = 4 deg). Each of these two FRFs had good coherence and are plotted in Fig. 15. Superimposed on the figure are discrete data points indicating the direct, elevon-induced torsion moments (previously shown in Figs. 9b and 9d). Figure 15 now makes it clear that the torsion response trends shown in Figs. 9b and 9d were caused by the torsion structural dynamics. Specifically, note how the 450 RPM data points increase with frequency as the torsion response begins to approach the resonant frequency. The amplitude changes for 760 RPM are similar but are larger since the integer harmonics at 760 RPM (1/rev - 5/rev) cover a wider range of frequencies than at 450 RPM. Note that for 760 RPM, the slight reduction in amplitude at 5/rev (relative to 4/rev) is explained by its distance from the torsional natural frequency. The offset between the discrete data points and the FRF for 760 RPM is simply caused by blade-to-blade differences. Specifically, elevon 1 was more effective than elevon 2; this difference was possibly caused by aerodynamic profile differences between the two active sections. Additional details are given in Ref. 8.

The corresponding flap bending moments are shown in Figs. 16 and 17 for 450 and 760 RPM, respectively. Figure 16 (450 RPM) shows a close agreement between the FRF and the discrete points (which were extracted from the phase sweeps). In fact, the FRF illuminates the cause of the trends previously shown in Fig. 9a – the maximum response is at 1/rev, the minimum is at 3/rev, and the remaining induced moments are of varying magnitudes; the magnitude of these responses are governed by their proximity to neighboring structural dynamic resonances and antiresonances. Similarly, the 760 RPM results in Fig. 17 explain why the 2/rev and 5/rev induced moments are significantly smaller than those at 3 and 4/rev. (Note that the FRF curve used for 760 RPM is approximated by hover at θ_o = 3.5 deg because of the coherence problems previously described for forward flight at this rotor speed.) The discrepancy at 1/rev is not fully understood but may be exacerbated by a difference between the hover and forward flight FRFs at low frequencies.

Finally, note the FRF spikes at some of the rotor harmonics, in particular the 2/rev spikes for 450 and 760 RPM (Figs. 16 and 17), as well as the 4/rev spike for the 450 RPM case (Fig. 16). Such spikes are typical of the FRF results and have a correspondingly low value of coherence. This "noise-to-signal" problem is inherent to the periodic forced vibratory response caused for forward flight (and even non-ideal hover). The "noise-to-signal" problem was reduced for the zero collective test condition shown in Figs. 14a and 14b. In general, if the excitation from the elevon is sufficiently large, the calculated FRFs will be accurate except near the harmonics of the rotor speed.

Implications for Future Testing

While the flap bending moment FRFs were acceptable in hover at 760 RPM (Ref. 8), those obtained in forward flight were not adequate. The strength of the FRF technique, however, suggests that it should be used in future tests; additional effort should be made to increase the flap bending moment coherence by increasing the amplitude of the elevon motion and/or increasing the length of the data records. In future

tests, near real-time processing techniques should be used to monitor the quality of the results.

Another future improvement would be to fit the FRFs with transfer functions or to use the FRFs for state space model identification; both modeling techniques are available from CIFER®, which uses optimization techniques that weigh the results based on the coherence and random error. Such techniques show promise for extracting the aeroelastic characteristics like elevon effectiveness, blade frequencies, and damping. Future work may include such calculations.

Concluding Remarks

1. A small-scale rotor open-loop test successfully demonstrated the effectiveness of on-blade elevon controls for significantly reducing blade root vibratory flap bending moments. Testing was performed at representative forward flight advance ratios up to 0.3 at reduced tip speeds and at low and moderate thrust conditions. Operation at a nominal (760 RPM) and a reduced rotor speed (450 RPM) indicated significant differences in elevon vibration reduction effectiveness resulting from different dynamic pressure and dynamic response characteristics at the two rotor speeds.

2. Although no attempt was made to introduce combinations of harmonic elevon excitation to simultaneously reduce multiple components of vibratory loads, the results suggest that appropriate control strategies could accomplish this objective.

3. The discrete harmonic phase sweep technique proved very successful in evaluating the effectiveness of on-blade elevons for changing the vibratory blade loads. In conjunction with an approximate but effective superposition model it was possible to identify the magnitude and phase of the elevon-induced moments for a range of rotor blade harmonic excitation frequencies.

4. The use of frequency sweep testing with CIFER® postprocessing was effective in determining the forward flight frequency response functions for elevon-induced blade loads, particularly at 450 RPM.

5. In general, the effects of increasing forward flight on the FRFs appeared as increased damping of the peak responses at resonant natural frequencies; for low frequencies (less than 5 Hz) the effects were similar to the variation of dynamic pressure with increased rotor speed; specifically, the torsion moment response increased with advance ratio and the flap bending moment response exhibited behavior characteristic of elevon reversal.

6. Both the frequency sweep and the discrete frequency phase sweep test methods were highly complementary and both measurements of the elevon effectiveness were in very good agreement. The two methods provide an opportunity to unify alternative views of rotor blade dynamic response – the continuous FRF description and traditional response characteristics at discrete rotor harmonics.

7. Comparison of the continuous FRFs and the discrete elevon-induced blade bending and torsion loads provides insights for structural dynamic tailoring to enhance loads reduction effectiveness of on-blade elevons.

8. A complete evaluation of the practical effectiveness and suitability of active on-blade elevon controls for fuselage vibration reduction will require additional testing with more sophisticated rotor models, measurement of rotor hub vibratory loads, concurrent evaluation with analytical models, and inclusion of closed loop active control systems.

References

1. Millott, T.A., and Friedmann, P.P., "Vibration Reduction in Helicopter Rotors Using an Active Control Surface Located on the Blade," AIAA-92-2451-CP, Proceedings of the 33rd AIAA/ASME/ASCE/AHS/ASC Structures, Structural Dynamics, and Materials Conference, Dallas, TX, April 13-15, 1992.

2. Millott, T.A., and Friedmann, P.P., "Vibration Reduction in Helicopter Rotors Using an Actively Controlled Partial Span Trailing Edge Flap Located on the Blade," NASA CR 4611, June 1994.

3. Milgram, and Chopra, I., "Helicopter Vibration Reduction with Trailing Edge Flaps," Proceedings of the American Helicopter Society Northeast Region Aeromechanics Specialists' Meeting, Stratford, CT, October 1995.

4. Milgram, J., and Chopra, I., "Dynamics of an Actively Controlled Plain Trailing Edge Flap System for a Modern Bearingless Rotor," Proceedings of the 23rd European Rotorcraft Forum, Dresden, Germany, September 16-18, 1997.

5. McCloud, J.L., III, and Weisbrich, A.L., "Wind Tunnel Test Results of a Full Scale Multi-cyclic Controllable Twist Rotor," Proceedings of the American Helicopter Society 34th Annual Forum, Washington, DC, May 15-17, 1978.

6. Wei, F.-S., and Weisbrich, A.L., "Multicyclic Controllable Twist Rotor Data Analysis," NASA CR 152251, January 1979.

7. Dawson, S., Hassan, A., Straub, F., and Tadghighi, H., "Blade-Mounted Flap Control for BVI Noise Reduction Proof-of-Concept Test," NASA CR 195078, July 1995.

8. Fulton, M.V., and Ormiston, R.A., "Hover Testing of a Small-Scale Rotor with On-Blade Elevons," Proceedings of the American Helicopter Society 53rd

Annual Forum, Virginia Beach, VA, April 29-May 1, 1997.

9. Rutkowski, M.J., Ruzicka, G.C., Ormiston, R.A., Saberi, H., and Jung, Y., "Comprehensive Aeromechanics Analysis of Complex Rotorcraft Using 2GCHAS," *Journal of the American Helicopter Society*, Vol. 40, (4), 1995.

10. Tischler, M.B., Cauffman, M.G., "Frequency-Response Method for Rotorcraft System Identification: Flight Applications to BO-105 Coupled Rotor/Fuselage Dynamics," *Journal of the American Helicopter Society*, Vol. 37, (3), 1992.

11. Tischler, M.B., Driscoll, J.T., Cauffman, M.G., and Freedman, C.J., "Study of Bearingless Main Rotor Dynamics from Frequency-Response Wind Tunnel Test Data," Presented at the American Helicopter Society Aeromechanics Specialists Conference, San Francisco, CA, January 19-21, 1994.

Table 1. Rotor Characteristics & Operating Conditions.

Description	Variable	Value
No. of Blades	b	2
Rotor Radius	R	45 in (3.75 ft)
Airfoil		NACA 0012
Airfoil Chord	c	3.4 in
Elevon Chord	c_{elv}	0.34 in (10% c)
Elevon Span	S_{elv}	5.55 in (12% R)
Solidity	σ	0.048
Lock No.	γ	5 - 7.5
Precone	β_o	0.0
Nominal Rotor Speed	Ω_o	760 RPM (12.7 Hz)
1st Flap Mode	$\omega_{\beta 1}$	1.11/rev*
1st Lag Mode	$\omega_{\zeta 1}$	1.08/rev*
1st Torsion Mode	$\omega_{\phi 1}$	4.6/rev*
Airspeed	V_{tip}, V_{elv}	298, 224 ft/s
Dynamic Pressure	q_{tip}, q_{elv}	106, 60 lb/ft^2
Reynolds Number	Re_{tip}, Re_{elv}	540,000; 400,000
Mach Number	M_{tip}, M_{elv}	0.27, 0.20

* θ_0=0 deg, 760 RPM, in air

Table 2. Collective pitch angles for elevon phase sweep test matrix at 760 RPM (0 deg shaft angle).

ω/μ	0.1	0.2	0.3
1		0°, 2°, 3°, 4°	
2		0°, 2°, 3°, 4°	
3	2°	0°, 2°, 3°, 4°	2°
4	2°, 3°	0°, 2°, 3°, 4°	2°, 3°
5	2°	0°, 2°, 3°, 4°	2°

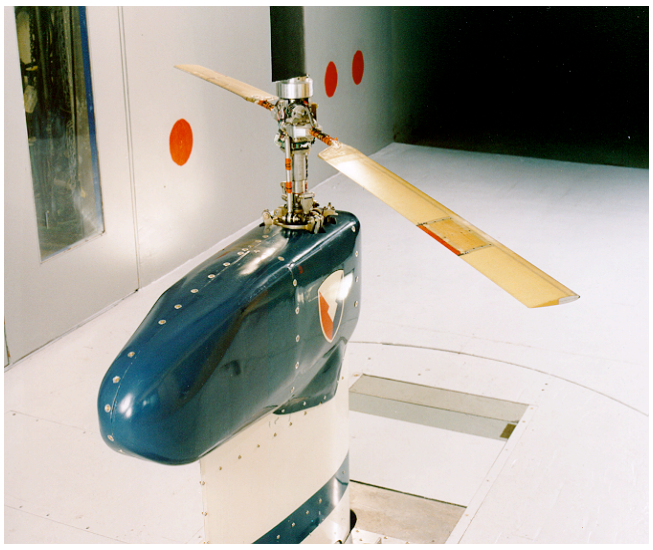

Fig. 1 Rotor with on-blade elevons in the Army/NASA 7- by 10-Ft. Wind Tunnel.

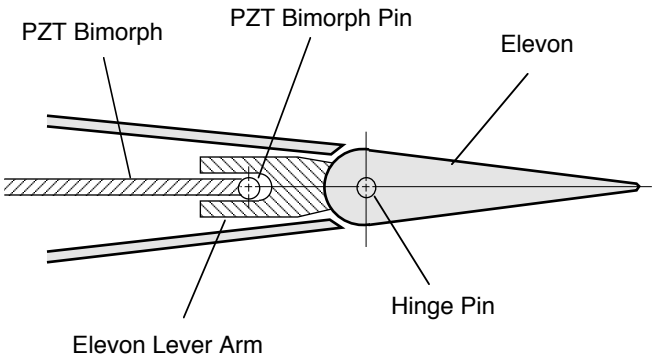

Fig. 2 Airfoil cross section, PZT bimorph bender beam and elevon lever arm mechanism.

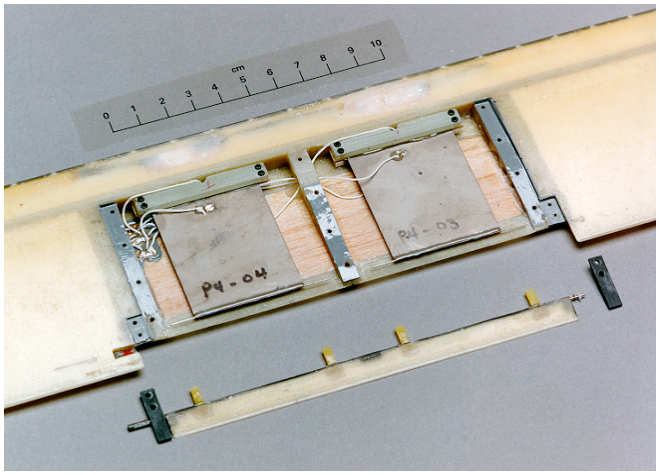

Fig. 3 Close-up of the active section with the access panel removed and the elevon disassembled.

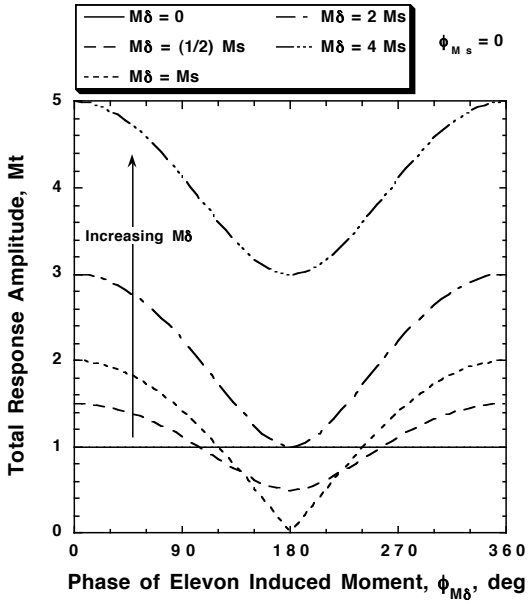

Fig. 5 Superposition model of sine wave summation – a plot of the total moment for various values of the elevon-induced moment.

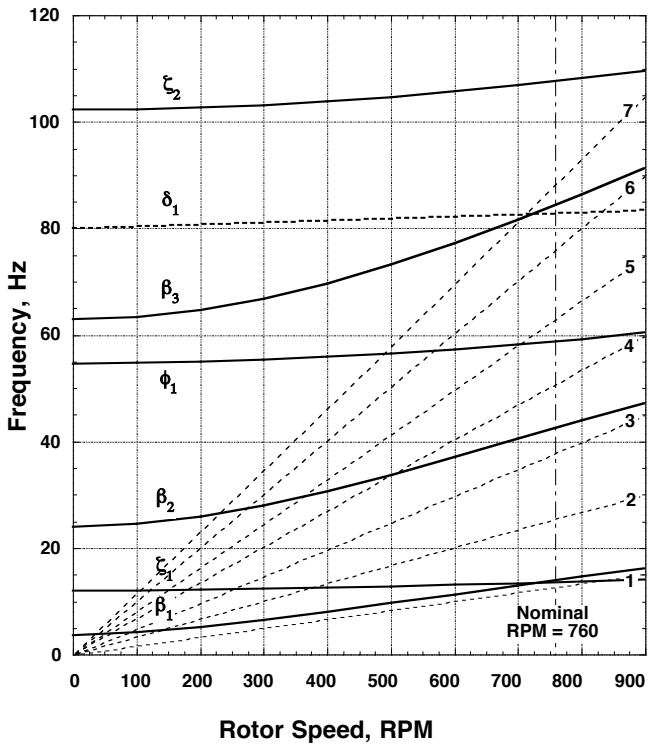

Fig. 4 Rotor blade frequencies versus rotor speed in air at zero collective pitch (β: flap, ζ: lead-lag, ϕ: torsion, δ: elevon angle).

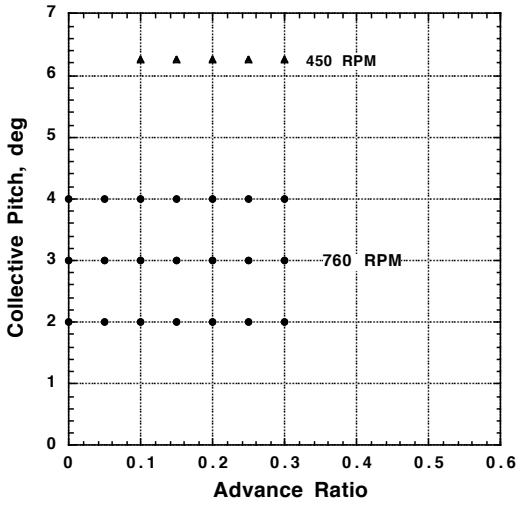

Fig. 6 Steady-state test matrix (760 and 450 RPM at 0 deg shaft angle).

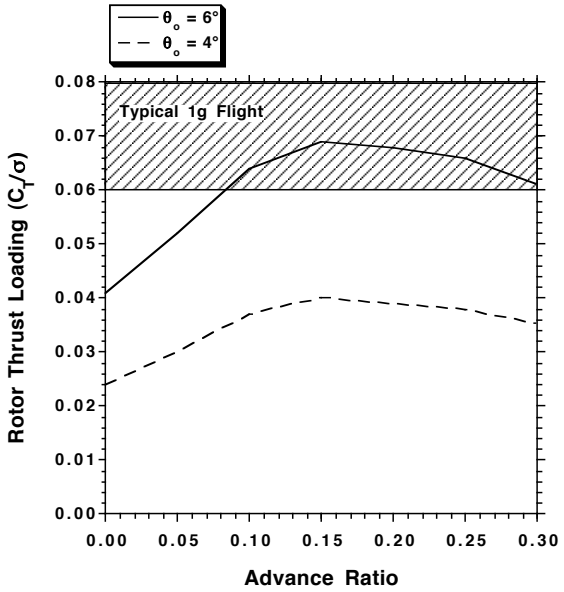

Fig. 7a Representative rotor thrust loading (760 RPM).

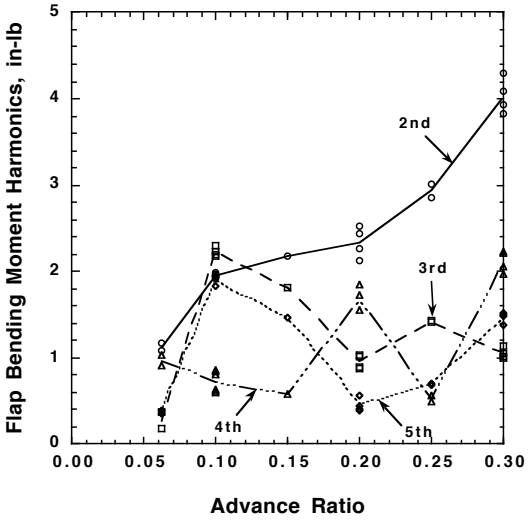

Fig. 7c Effect of advance ratio on baseline steady-state flap bending moment harmonics at 450 RPM (θ_o = 6.25 deg, blade 1).

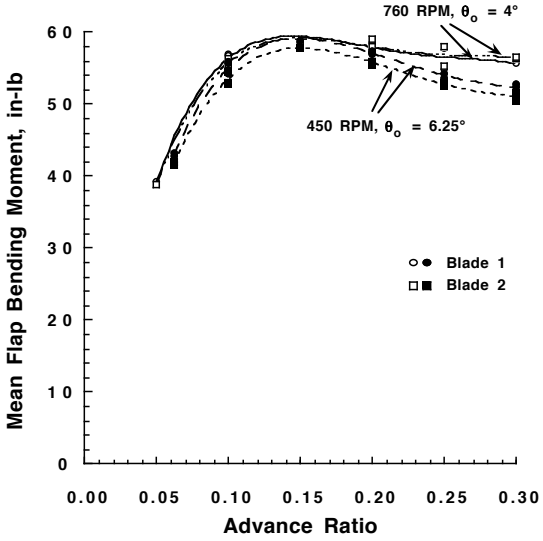

Fig. 7b Variation of mean flap bending moment with advance ratio at two flight conditions (blades 1 and 2).

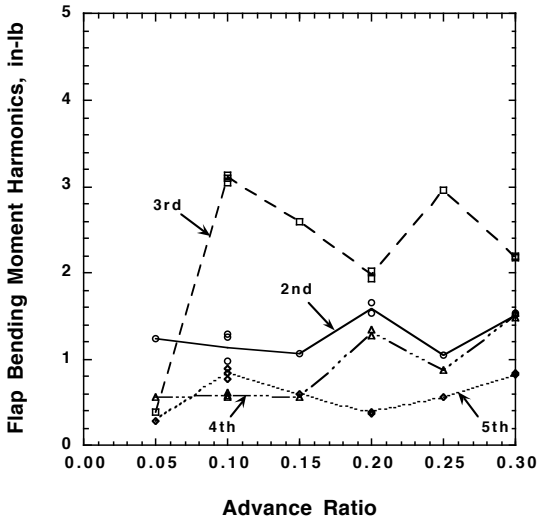

Fig. 7d Effect of advance ratio on baseline steady-state flap bending moment harmonics at 760 RPM (θ_o = 4 deg, blade 1).

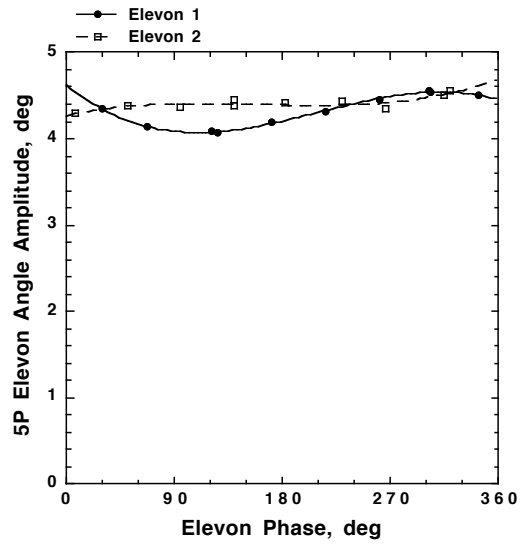

Fig. 8a Relative insensitivity of 5/rev elevon motion to elevon phase (75 Vrms 5/rev PZT voltage, 760 RPM, $\theta_o = 4$ deg, $\mu = 0.2$).

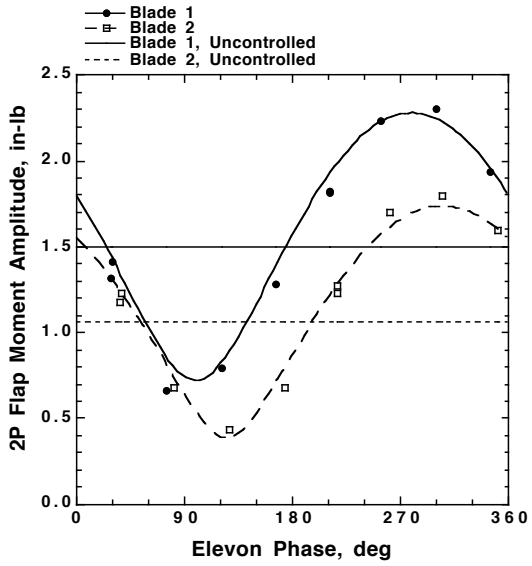

Fig. 8c Variation of 2/rev flap bending moment with elevon phase (110 Vrms 2/rev PZT voltage, 760 RPM, $\theta_o = 4$ deg, $\mu = 0.2$).

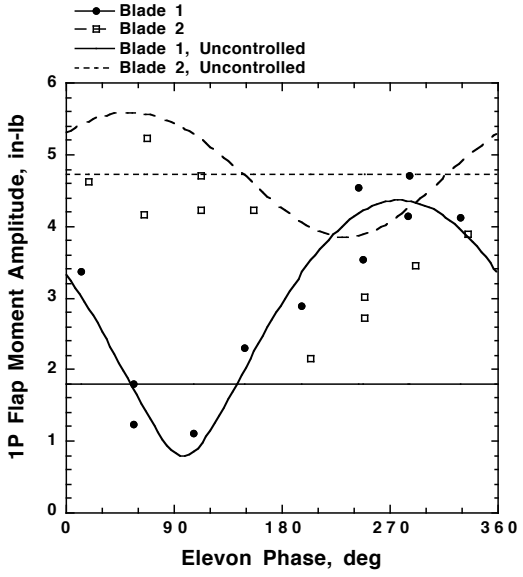

Fig. 8b Variation of 1/rev flap bending moment with elevon phase (110 Vrms 1/rev PZT voltage, 760 RPM, $\theta_o = 4$ deg, $\mu = 0.2$).

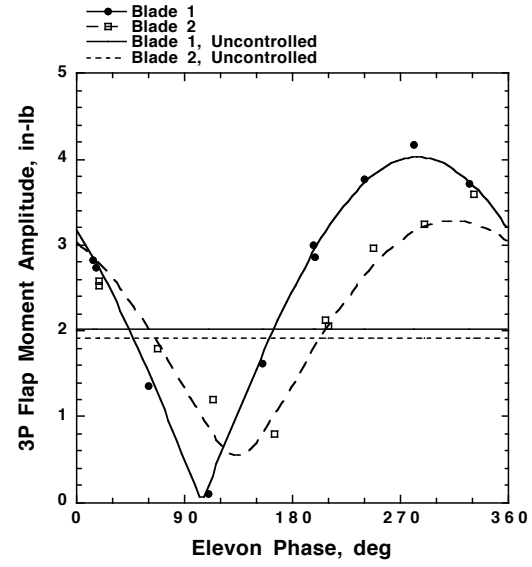

Fig. 8d Variation of 3/rev flap bending moment with elevon phase (75 Vrms 3/rev PZT voltage, 760 RPM, $\theta_o = 4$ deg, $\mu = 0.2$).

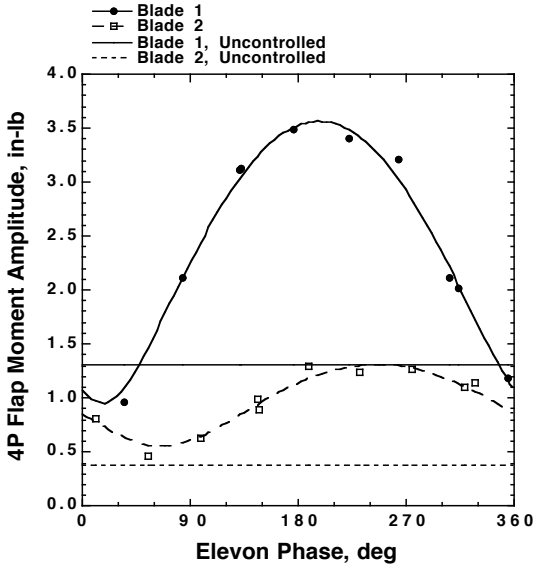

Fig. 8e Variation of 4/rev flap bending moment with elevon phase (66 Vrms 4/rev PZT voltage, 760 RPM, θ_o = 4 deg, μ = 0.2).

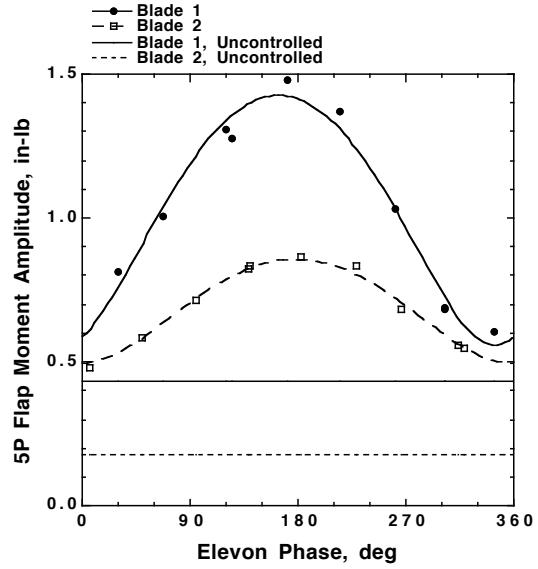

Fig. 8f Variation of 5/rev flap bending moment with elevon phase (75 Vrms 5/rev PZT voltage, 760 RPM, θ_o = 4 deg, μ = 0.2).

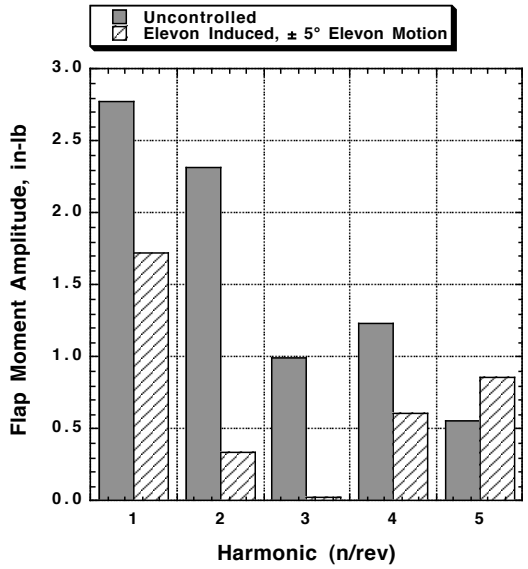

Fig. 9a Uncontrolled and elevon-induced flap bending moment harmonics (450 RPM, θ_o = 6.25 deg, μ = 0.2, ± 5 deg elevon motion, blade 1).

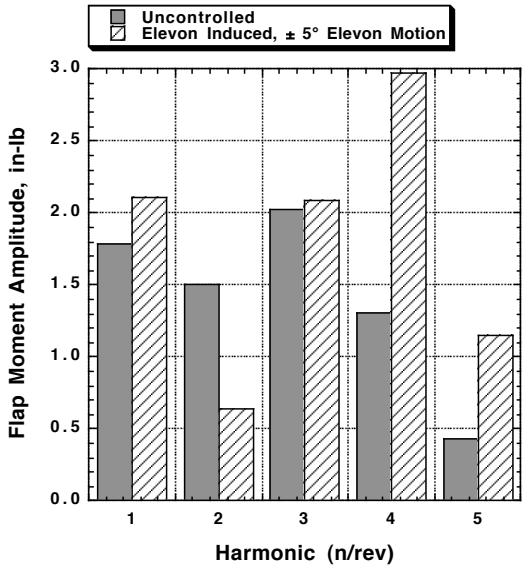

Fig. 9c Uncontrolled and elevon-induced flap bending moment harmonics (760 RPM, θ_o = 4 deg, μ = 0.2, ± 5 deg elevon motion, blade 1).

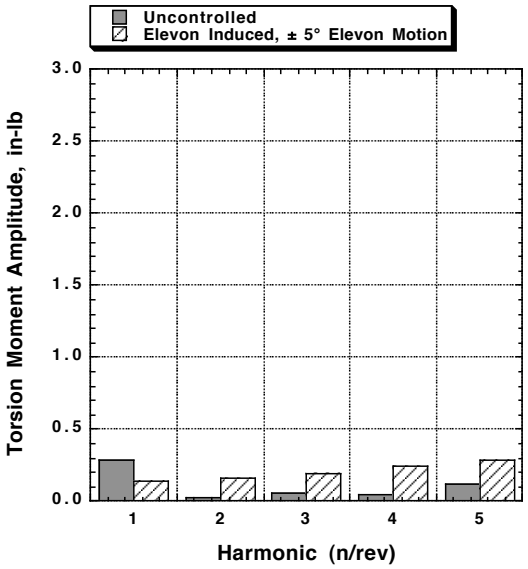

Fig. 9b Uncontrolled and elevon-induced torsion moment harmonics (450 RPM, θ_o = 6.25 deg, μ = 0.2, ± 5 deg elevon motion, blade 1).

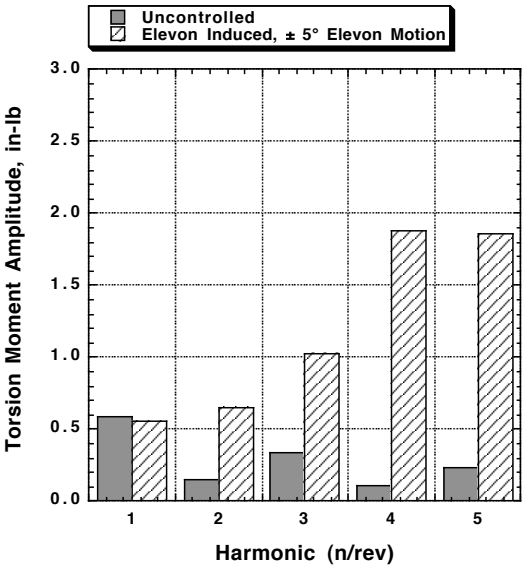

Fig. 9d Uncontrolled and elevon-induced torsion moment harmonics (760 RPM, θ_o = 4 deg, μ = 0.2, ± 5 deg elevon motion, blade 1).

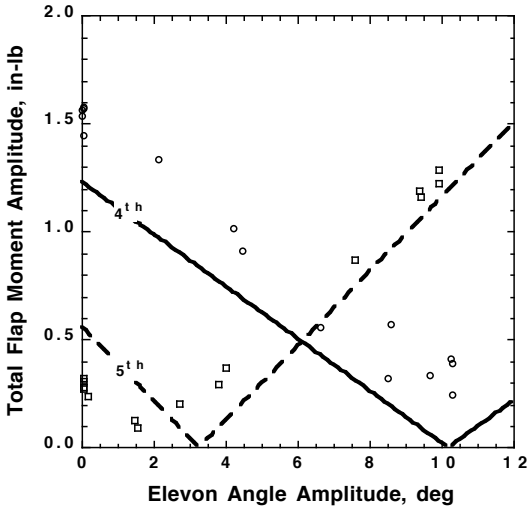

Fig. 10a Effect of elevon excitation amplitude on flap bending moment harmonics; derived from experimental measurements (450 RPM, θ_o = 6.25 deg, μ = 0.2, blade 1).

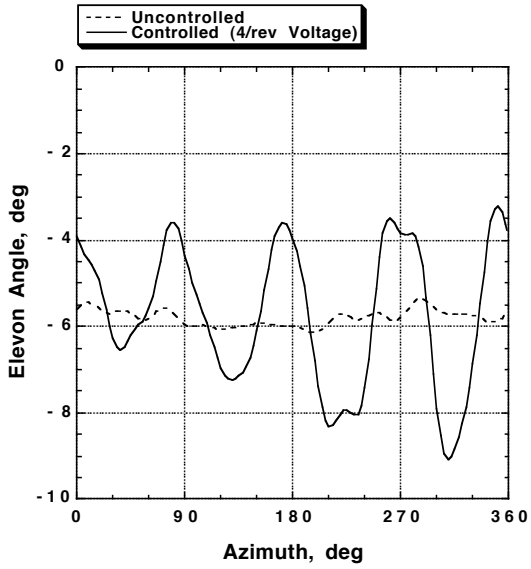

Fig. 11 Elevon motion over one rotor revolution for two cases, one with 42.6 Vrms 4/rev PZT voltage and the other zero applied voltage (760 RPM, θ_o = 4 deg, μ = 0.2, blade 1).

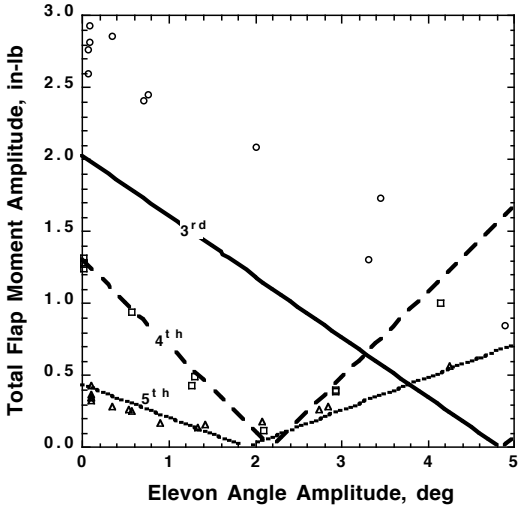

Fig. 10b Effect of elevon excitation amplitude on flap bending moment harmonics; derived from experimental measurements (760 RPM, θ_o = 4 deg, μ = 0.2, blade 1).

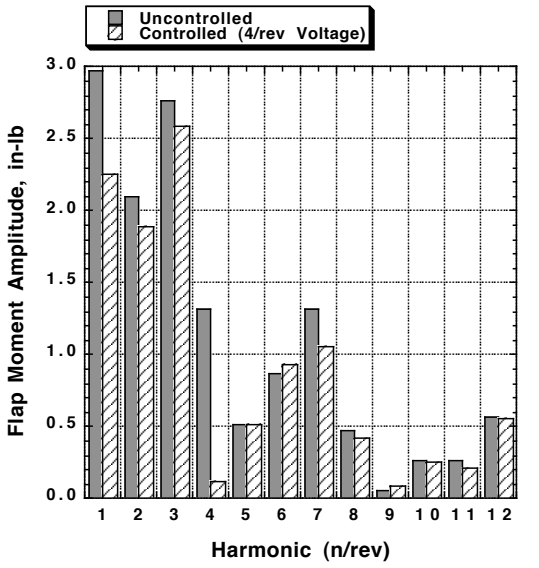

Fig. 12 Comparison of flap bending moment amplitudes with and without 4/rev elevon motion (uncontrolled: 0 Vrms, controlled: 42.6 Vrms; 760 RPM, θ_o = 4 deg, μ = 0.2, blade 1).

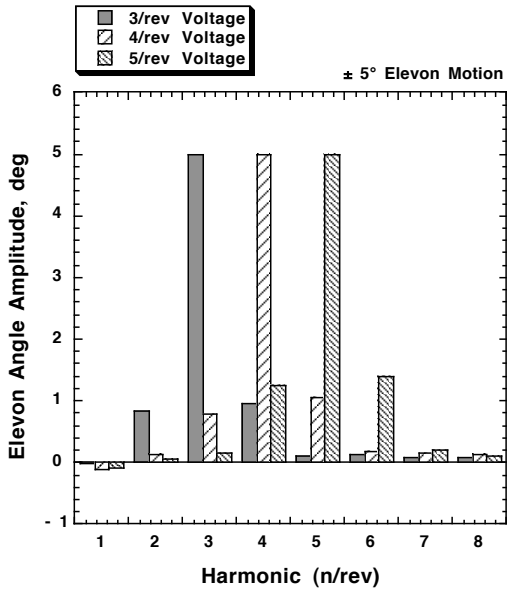

Fig. 13a Amplitude of elevon motion at primary and side harmonics of excitation voltage frequency for three excitation harmonics (760 RPM, θ_o = 2 deg, μ = 0.3, ± 5 deg elevon motion, blade 1).

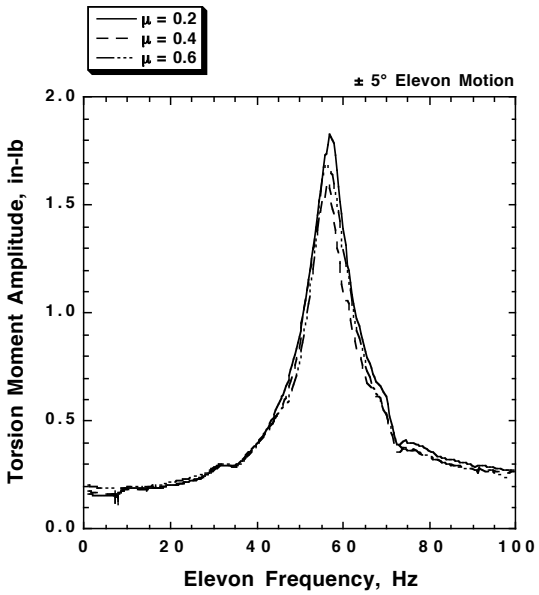

Fig. 14a Effect of advance ratio on torsion frequency response function for ± 5 deg elevon motion (450 RPM, θ_o = 0 deg, average results).

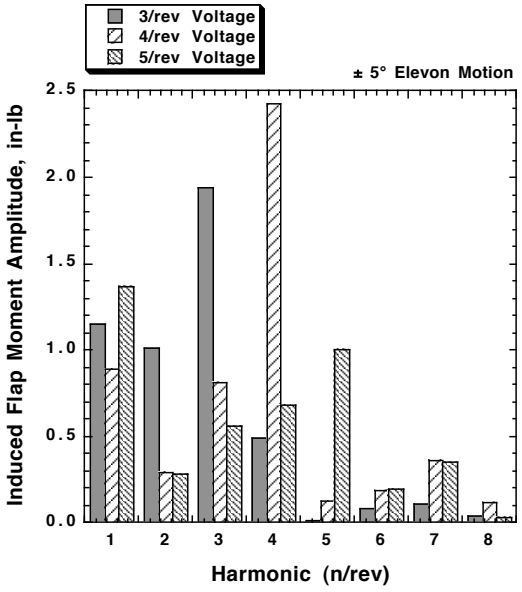

Fig. 13b Amplitude of induced flap moment at primary and side harmonics of excitation voltage frequency for three excitation harmonics (760 RPM, θ_o = 2 deg, μ = 0.3, ± 5 deg elevon motion, blade 1).

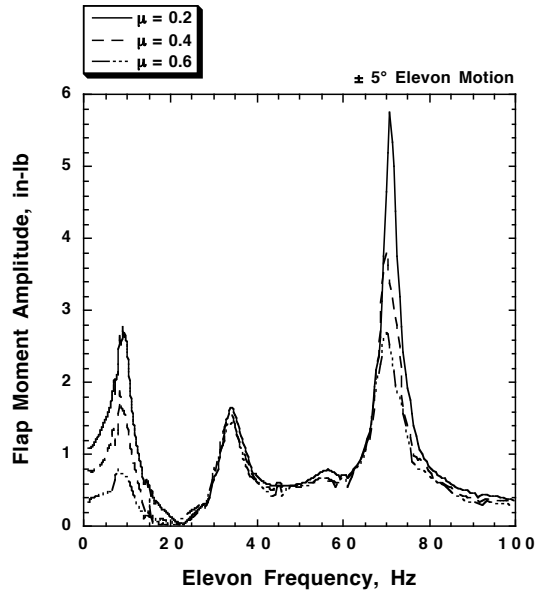

Fig. 14b Effect of advance ratio on flap bending moment frequency response function for ± 5 deg elevon motion (450 RPM, θ_o = 0 deg, ± 5 deg elevon motion, average results).

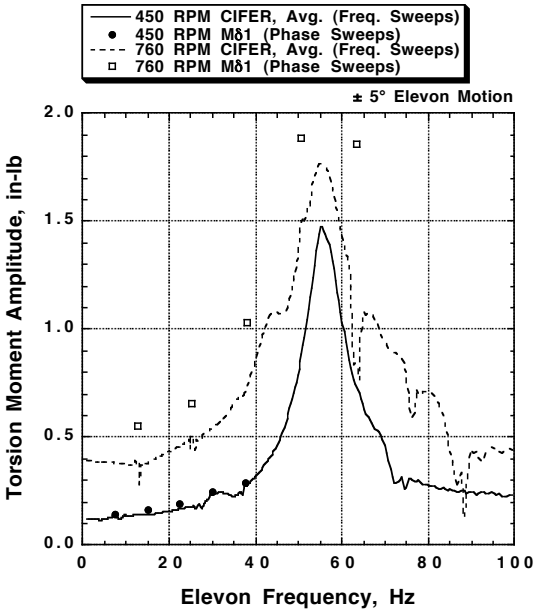

Fig. 15 Comparison of elevon-induced torsion moments (from phase sweeps) with frequency response functions for two rotor speeds (450 RPM at θ_o = 6.25 deg; 760 RPM at θ_o = 4 deg; μ = 0.2; ± 5 deg elevon motion; average and blade 1 results).

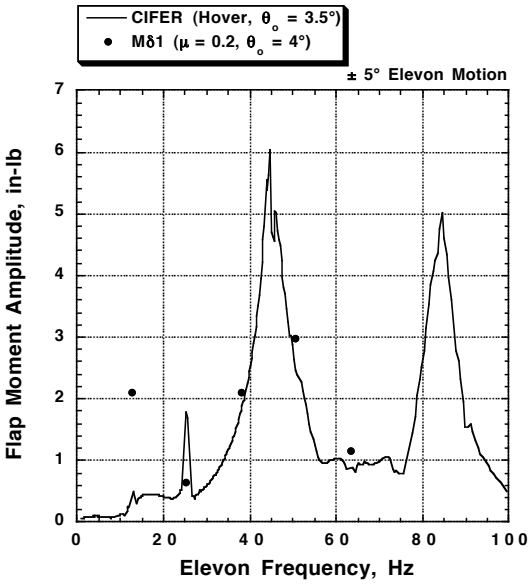

Fig. 17 Comparison of elevon-induced flap bending moments (from phase sweeps) with frequency response functions (760 RPM, θ_o = 3.5 - 4 deg, hover and μ = 0.2, ± 5 deg elevon motion, average and blade 1 results).

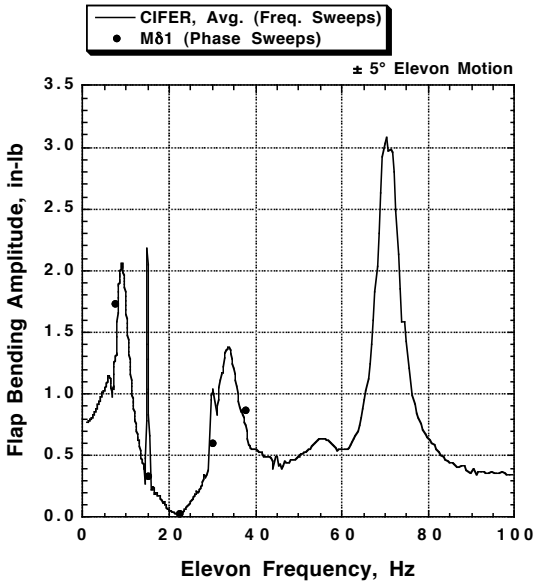

Fig. 16 Comparison of elevon-induced flap bending moments (from phase sweeps) with frequency response functions (450 RPM, θ_o = 6.25 deg, μ = 0.2, ± 5 deg elevon motion, average and blade 1 results).